

Supporting Information

Trimetallic Hollow Pt-Ni-Co Nanodendrites as Efficient Anodic Electrocatalysts

Rinrada Sriphathoorat,[†] Kai Wang,[†] and Pei Kang Shen^{*,†,§}

[†] School of Materials Science and Engineering, Sun Yat-sen University, Guangzhou 510275, P. R. China

[§] Collaborative Innovation Center of Sustainable Energy Materials, Guangxi Key Laboratory of Electrochemical Energy Materials, State Key Laboratory of Processing for Non-Ferrous Metal and Featured Materials, Guangxi University, Nanning 530004, P. R. China. *E-mail: pkshen@gxu.edu.cn

Experimental Section

Materials: Chloroplatinic acid hexahydrate ($\text{H}_2\text{PtCl}_6 \cdot 6\text{H}_2\text{O}$), cobalt(III) acetylacetonate [$\text{Co}(\text{acac})_3$, 97%], nickel(II) acetate [$\text{Ni}(\text{CH}_3\text{COO})_2 \cdot 4\text{H}_2\text{O}$, 98%], cetyltrimethylammonium chloride (CTAC, 97%), oleylamine (OAm, 80–90%) and n, n-dimethylformamide (DMF, 99.5%) were purchased from Aladdin. Solvents such as hexane, ethanol, methanol, and acetic acid were analytical grade. All chemicals were used without further purification. Ultrapure (18.2 M Ω) water and ethanol were used to clean all glasswares and autoclaves in the experiments.

Synthesis of Pt-Ni-Co nanodendrites: In a typical synthesis, 0.32 ml of H_2PtCl_6 , 6.2 mg of $\text{Co}(\text{acac})_3$, 39.0 mg of $\text{Ni}(\text{CH}_3\text{COO})_2$, and 164.0 mg of CTAC were dissolved in mixed solution containing 8 ml of OAm and 2 ml of DMF. After ultrasonication 30 minutes, the homogeneous solution in sealed autoclave was heated at 170 °C and kept at this temperature for 12 hours, then naturally cooled down to room temperature. The resulting colloidal product was washed twice with ethanol, and collected by centrifugation 4,000 rpm for 5 minutes.

Chemical corrosion of solid Pt-Ni-Co nanodendrites to hollow structure: 10 ml of acetic acid is added to Pt-Ni-Co nanodendrites. The suspension was ultrasonicated for 10 minutes, then heated at 70 °C for 12 hours. After corrosion, the product was washed three times with ethanol, and collected by centrifugation.

Preparation and activation of carbon-supported catalysts: In a typical preparation, carbon powder (Vulcant-72) and Pt-Ni-Co nanocrystals were dispersed in 20 ml of n-butylamine. The mixture was ultrasonicated for 1 hour, then stirred at room temperature for 72 hours. The product was washed twice with methanol and once with ethanol to remove the excess n-butylamine. The final product was collected by centrifugation, and dried at 80 °C in vacuum oven overnight. Before using as electrocatalysts, the sample was heated in furnace at 200 °C for 1 hour, then naturally cooled down to room temperature. The thermal treatment was carried out to remove residual organic compounds such as oleylamine or CTAC and anneal the catalysts for catalytic reaction.

Material characterization: Transmission electron microscopy (TEM) and energy dispersive spectroscopy (EDS) were performed with a FEI Tecnai G2 Spirit transmission electron microscope operating at 120 kV. High-resolution transmission electron microscopy (HR-TEM), high-angle annular dark-field scanning transmission electron microscopy (HAADF-STEM), and EDS mapping were performed with a FEI Tecnai G2 F-30 transmission electron microscope. The samples were prepared by dropping hexane dispersion of catalysts on 300-mesh grids. The powder X-ray diffraction (XRD) patterns were recorded with a Rigaku D-MAX 200 VPC X-ray diffractometer with Cu K α radiation ($\lambda = 1.54056 \text{ \AA}$). The Pt loading was determined by inductively coupled plasma atomic emission spectroscopy (TJA RADIAL IRIS 1000 ICP-AES, USA).

Electrochemical measurements: The electrochemical measurements were conducted in a three-electrode cell with a PINE Computer-Controlled Bipotentiostat at 30 °C. A glassy-carbon rotating disk electrode (RDE) (diameter: 5 mm, area: 0.196 cm²) from Pine Instruments was used as the working electrode. A saturated calomel electrode (SCE) and a carbon rod were used as

reference and counter electrodes, respectively. Before the measurements, the catalysts were supported on commercial carbon powder to avoid agglomeration. The catalyst ink was prepared by homogeneously dispersing 2.0 mg of carbon-supported catalysts in a solution mixture containing 1.8 mL of absolute ethanol and 0.2 mL of 0.5 wt% Nafion solution (DuPont, USA), followed by ultrasonication for 30 minutes. The electrochemical active surface area (ECSA) were calculated by integrating the hydrogen adsorption charge with cyclic voltammetry (CV) carried out at room temperature in N₂ saturated 0.5 M H₂SO₄ solution. For the activity of methanol oxidation and formic acid oxidation, the CV profiles were recorded in 0.5 M H₂SO₄ + 1.0 M CH₃OH and 0.5 M H₂SO₄ + 0.25 M HCOOH, respectively. For the CO-stripping experiment, CO was purged into 0.5 M H₂SO₄ solution for 15 minutes, while the working electrode was held at -0.14 V vs. SCE. All CV profiles were recorded at a sweep rate of 50 mV s⁻¹ in a potential window between -0.2 and 1.0 V vs. SCE.

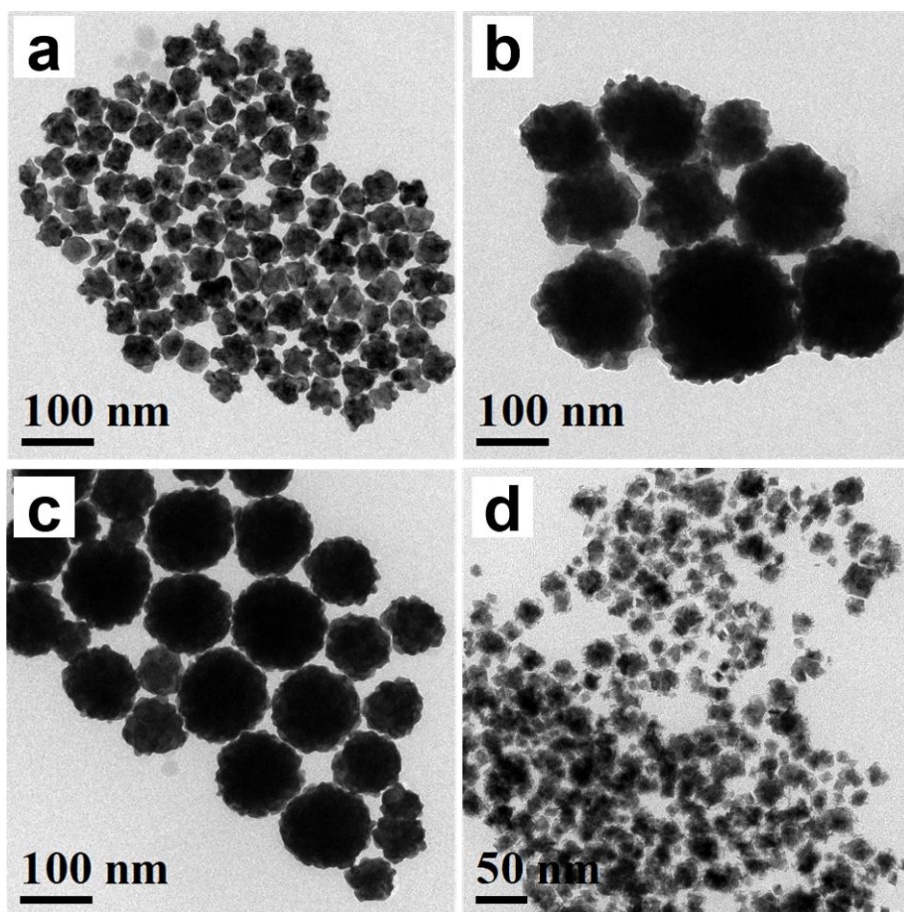


Figure S1. TEM images of the nanocrystals collected in different fraction of DMF: (a) 40%, (b) 60%, (c) 80% and (d) 100%.

The mixed solution of OAm/DMF was used to adjust morphology of Pt-Ni-Co nanocrystals. However, it was found that only OAm cannot yield solid Pt-Ni-Co NDs and no any nanocrystals were obtained in this condition. The introduction of DMF can promote reduction ability of the whole system, resulting the formation of Pt-Ni-Co nanoalloy. In present system, the little amount of DMF (20%) in solution were used to synthesize solid Pt-Ni-Co NDs. When amount of DMF increase to 40%, most of nanocrystals possess the rounded shape and some of them display branched structure (figure S1a). With increasing DMF to 60% and 80%, it results heavily aggregated particle (figure S1b and c). However, in the system without OAm, Co precursor cannot be reduced and alloyed, resulting Pt-Ni nanocrystals (figure S1d). Therefore, an appropriate fraction of OAm/DMF is essential for fabrication of solid Pt-Ni-Co NDs.

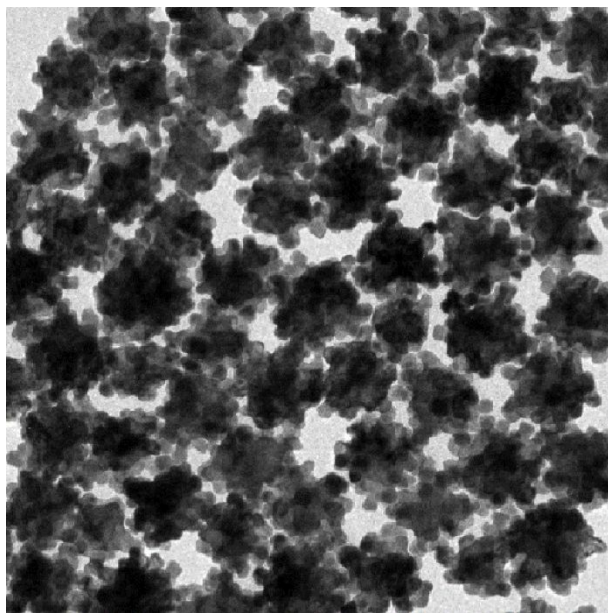


Figure S2. Low-magnificent TEM image of solid Pt-Ni-Co NDs.

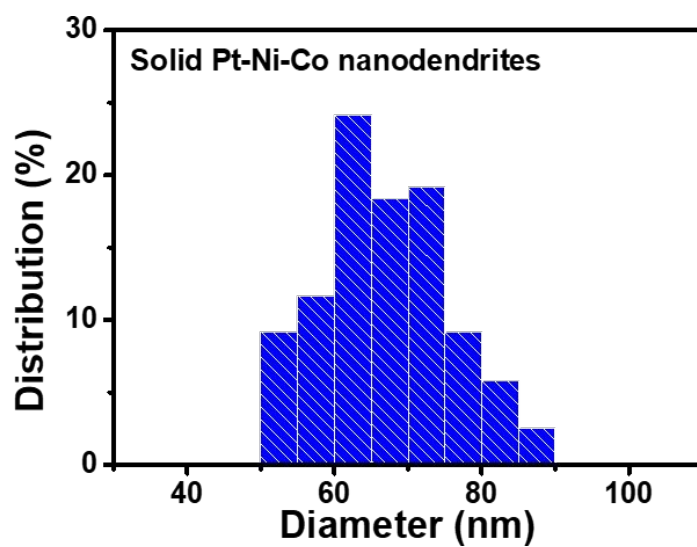


Figure S3. The particle size distribution of solid Pt-Ni-Co NDs

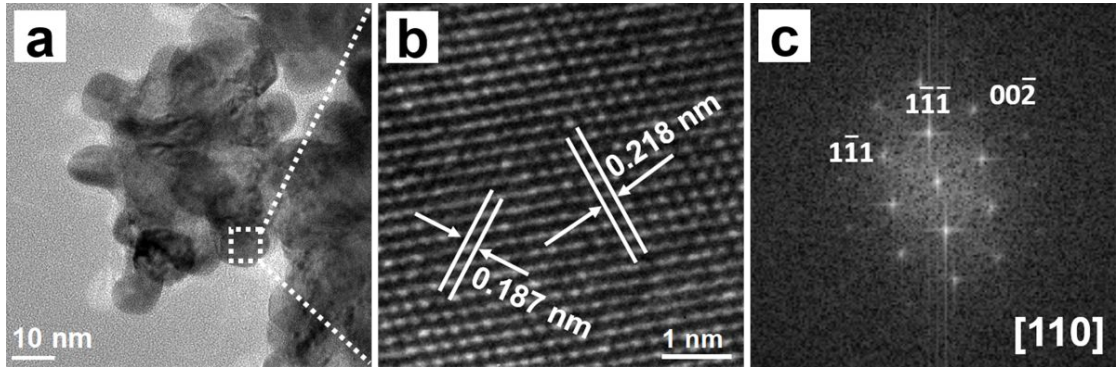


Figure S4. (a) HRTEM image, (b) enlarge selected area of solid Pt-Ni-Co NDs corresponding with (c) fast Fourier transform (FFT) pattern.

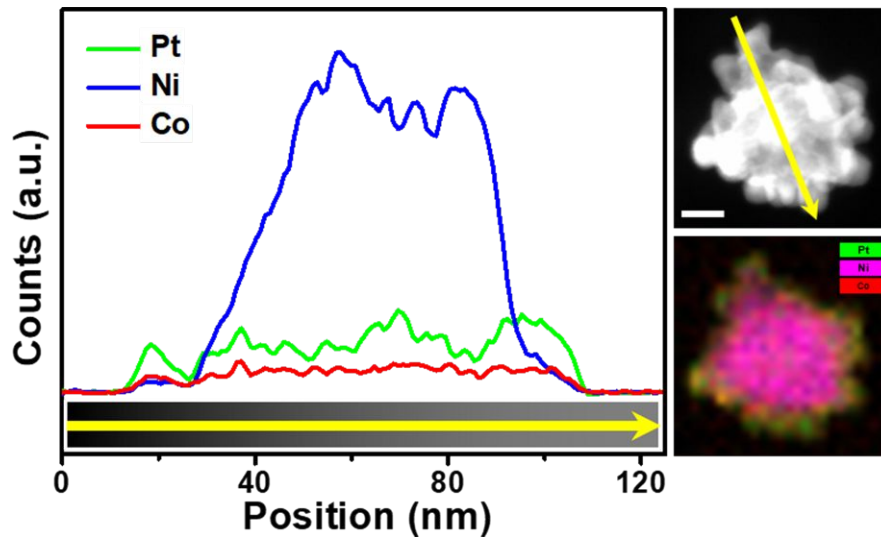


Figure S5. Line scanning profile of solid Pt-Ni-Co NDs.

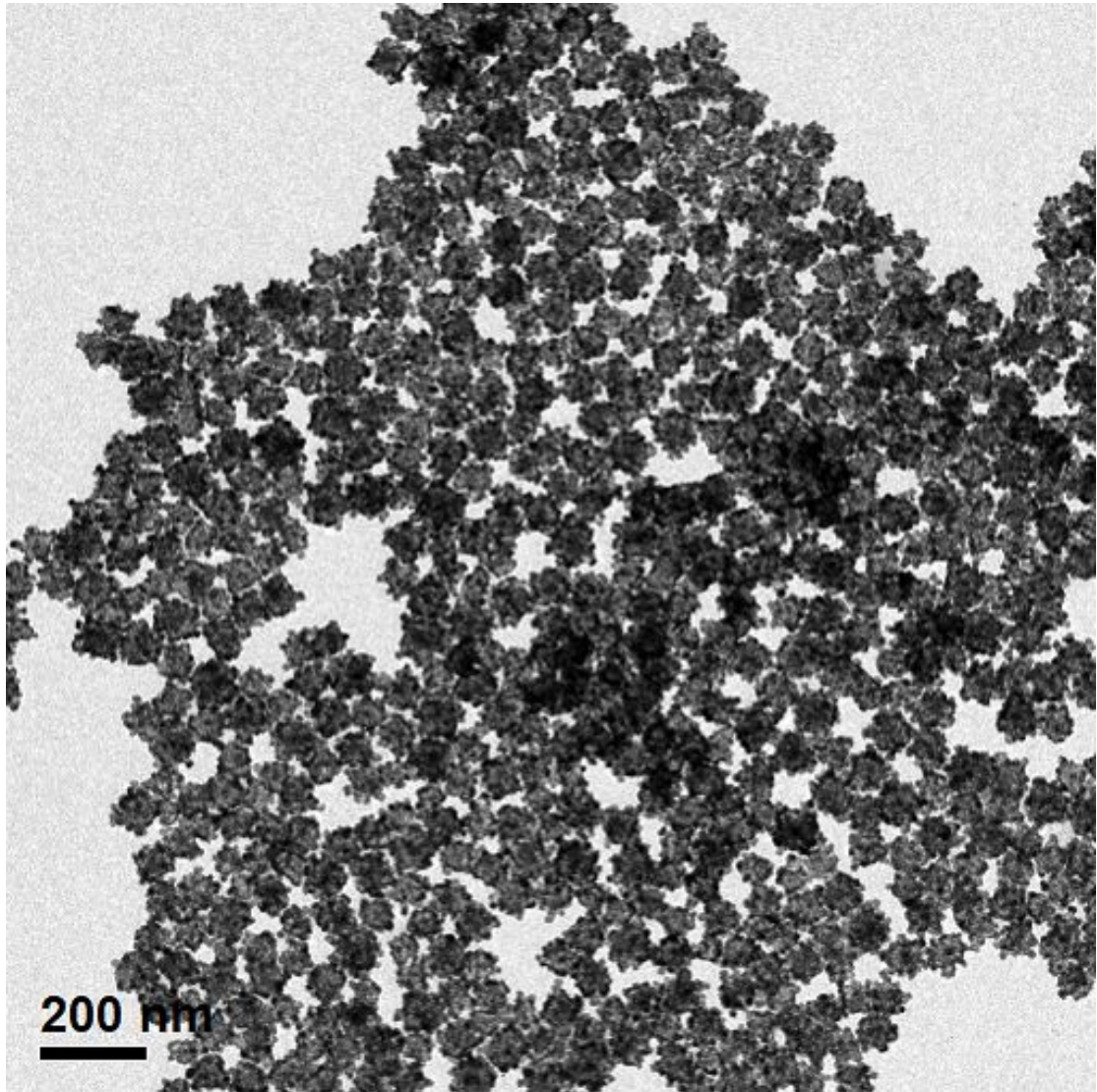


Figure S6. Large-area TEM image of hollow Pt-Ni-Co NDs

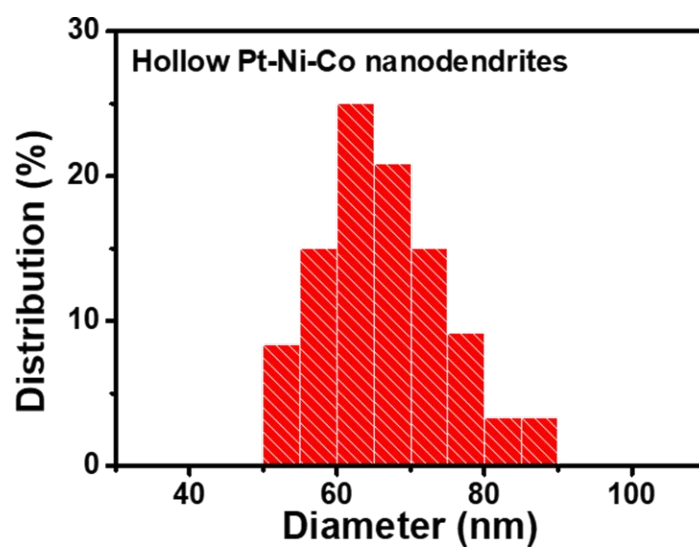


Figure S7. The particle size distribution of hollow Pt-Ni-Co NDs.

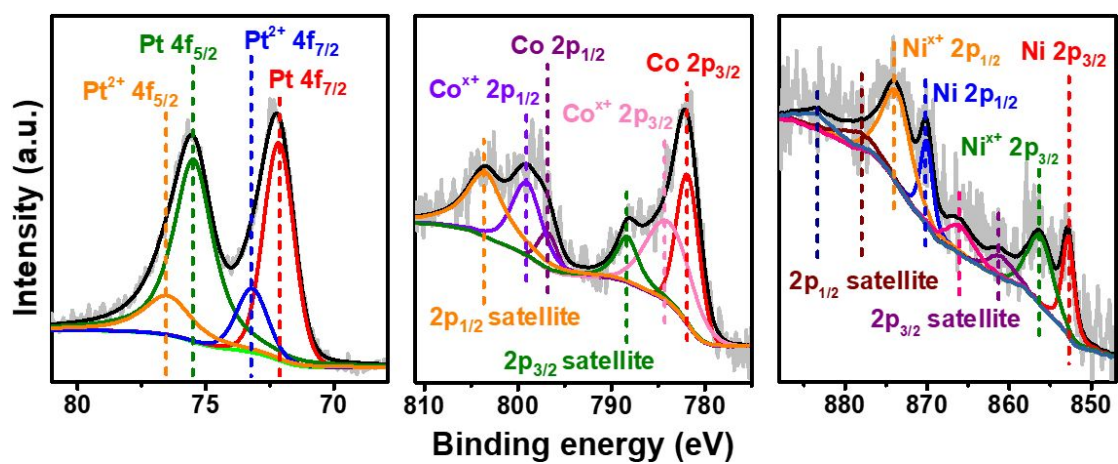


Figure S8. Pt 4f, Co 2p, and Ni 2p XPS spectra of hollow Pt-Ni-Co NDs.

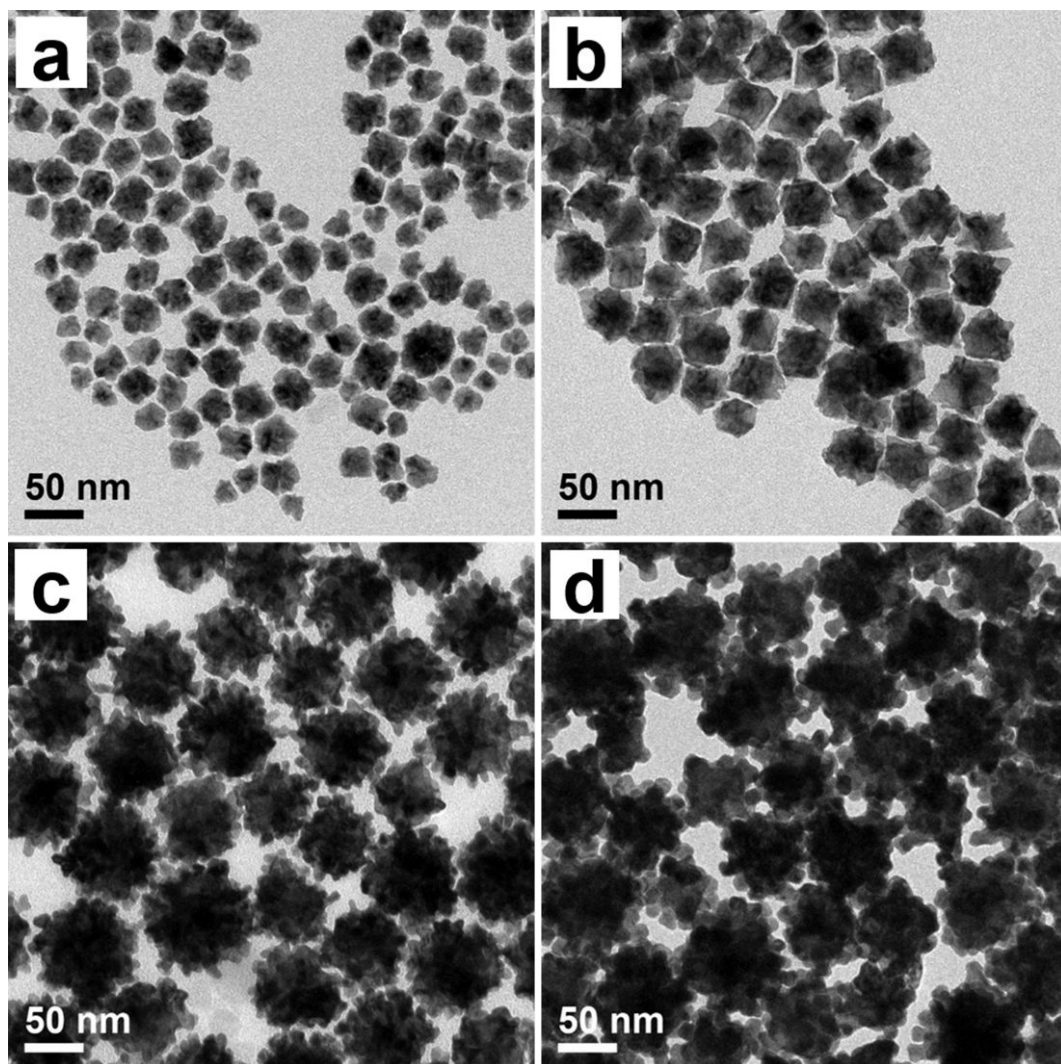


Figure S9. TEM images of the products collected at different reaction time: (a) 25 min, (b) 1 hr, (c) 2 hr, and (d) 12 hr.

At 25 minutes (figure S9a), most nanoparticles are small irregular shape with average particle size of 25 nm. When extending reaction time to 1 hour (figure S9b), some nanocrystals show branched structure and their average size increases to 38 nm. As the reaction time reached 2 hours (figure S9c), all nanocrystals obviously show branched structure with an average size of 58 nm. When increasing growth time from 2 to 12 hours, NDs are obtained while the size increased to about 66 nm.

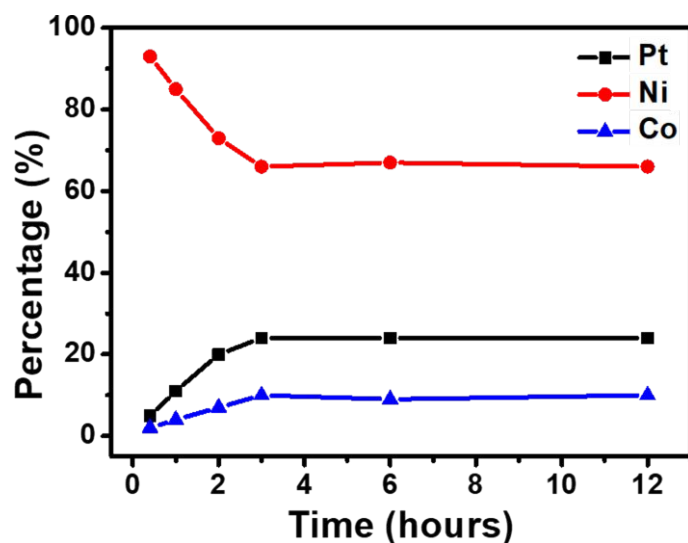


Figure S10. Correlation between Pt, Ni and Co content and reaction time during growth process.

The growth mechanism of solid Pt-Ni-Co NDs

The H_2PtCl_6 and Ni^{2+} might interact with CTAC dissolved in OAm via electrostatic attraction and chelate effect, which would weaken the contact of H_2PtCl_6 and OAm (as the reducing agent) and reduce the decomposition rates of H_2PtCl_6 .¹⁻⁴ Therefore, the Ni^{2+} was preferential reduced and lead to the formation of Ni-rich core.

During the formation of Pt-Ni-Co NDs, CTAC molecules would selectively absorb onto the {110} facets of nanocrystals, and while the oxidative etching caused by Cl^-/O_2 etchant would lead to the oxidation of some Ni atoms, which would facilitate the deposition of Pt atoms onto these area and grow into branched shape.⁵ Meanwhile, Co^{3+} would be reduced to Co^{2+} ($\text{Co}^{3+}/\text{Co}^{2+}$, 1.81 V) by OAm, followed by the reduction of Co^{2+} to Co (Co^{2+}/Co , -0.28 V), and then be incorporated into the nanocrystals,⁶ resulting the formation of core-shell Pt-Ni-Co NDs. In addition, the CTA^+ (released from CTAC) behaves the vital role to uniformly disperse nanocrystals because of its long alkyl chain, leading to form well-dispersed Pt-Ni-Co NDs.⁷

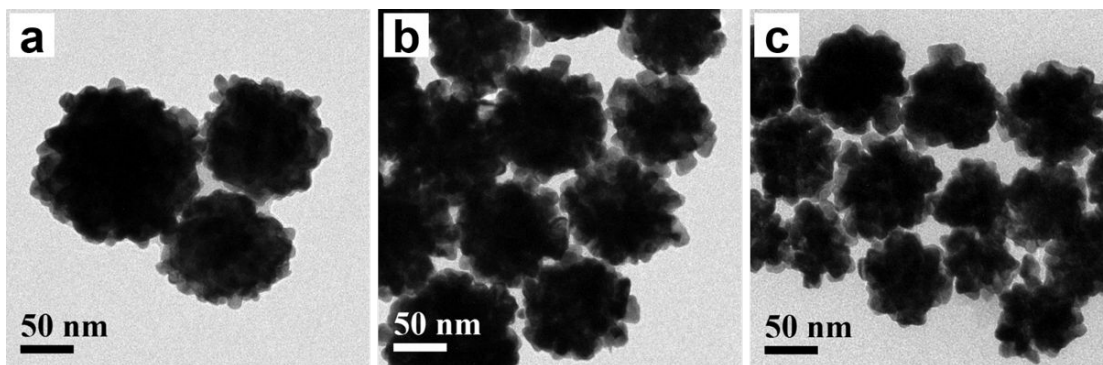


Figure S11. TEM images of products synthesized with (a) 64.0 mg Ni precursors, (b) 12.7 mg Ni precursors, and (c) 4.3 mg Ni precursors.

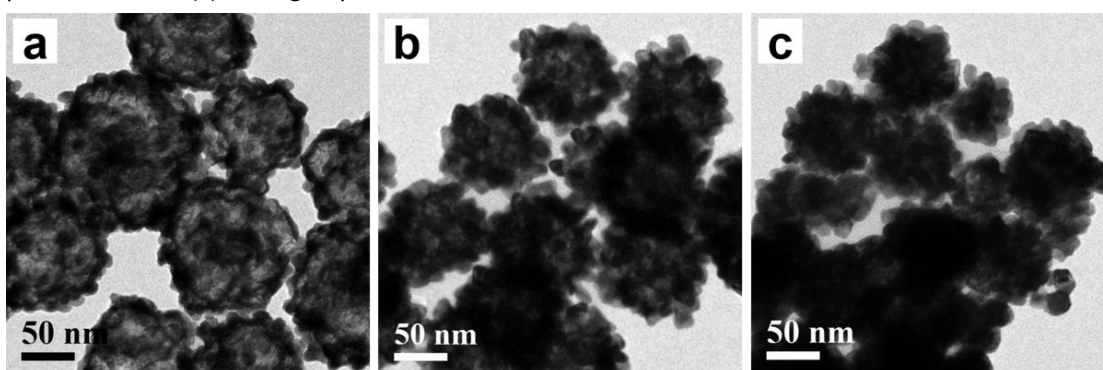


Figure S12. TEM images of products obtained after acid treatment. (a) $\text{Pt}_{18}\text{Ni}_{76}\text{Co}_6$ -AT, (b) $\text{Pt}_{41}\text{Ni}_{44}\text{Co}_{15}$ -AT, and (c) $\text{Pt}_{62}\text{Ni}_{17}\text{Co}_{21}$ -AT.

Importantly, amount of Ni precursors introduced into the system is a main factor to control opened structure. A series of experiment was carried out by varying amount of Ni precursors, while other conditions were kept constant. When Ni precursor increases to 64 mg, rough surface of $\text{Pt}_{18}\text{Ni}_{76}\text{Co}_6$ with the average size of 124 nm is obtained (figure S11a). When Ni precursor decreases to 12.7 mg (figure S11b), the synthesized nanocrystals also display nanodendrites with average size of 100 nm and their elemental composition are $\text{Pt}_{41}\text{Ni}_{44}\text{Co}_{15}$. Figure S11c is the TEM image of nanocrystals obtained when Ni precursor decreases to 4.3 mg, which show dendritic sphere of $\text{Pt}_{62}\text{Ni}_{17}\text{Co}_{21}$ with average size of 81 nm. After acetic acid treatment of the solid NDs in different atomic ratio, the resulting nanocrystals exhibit different opened structure, denoted as $\text{Pt}_{18}\text{Ni}_{76}\text{Co}_6$ -AT, $\text{Pt}_{41}\text{Ni}_{44}\text{Co}_{15}$ -AT, and $\text{Pt}_{62}\text{Ni}_{17}\text{Co}_{21}$ -AT. As shown in figure S12a, $\text{Pt}_{18}\text{Ni}_{76}\text{Co}_6$ -AT obviously processes large hollow structure with thin shell, while $\text{Pt}_{41}\text{Ni}_{44}\text{Co}_{15}$ -AT (figure S12b) show a smaller hollow degree. For $\text{Pt}_{62}\text{Ni}_{17}\text{Co}_{21}$ -AT (figure S12c), the nanocrystals show small void at center of nanoparticle. It is found that amount of Ni, which was reduced and formed in the core area, influences the hollow degree of nanocrystals. In other words, the hollow degree of nanocrystals can increase by decreasing the atomic ratio of Pt/Ni precursors. From this experiment, the opened structure of Pt-Ni-Co nanocrystals could be designed and controlled by changing the feeding amount of Ni precursor.

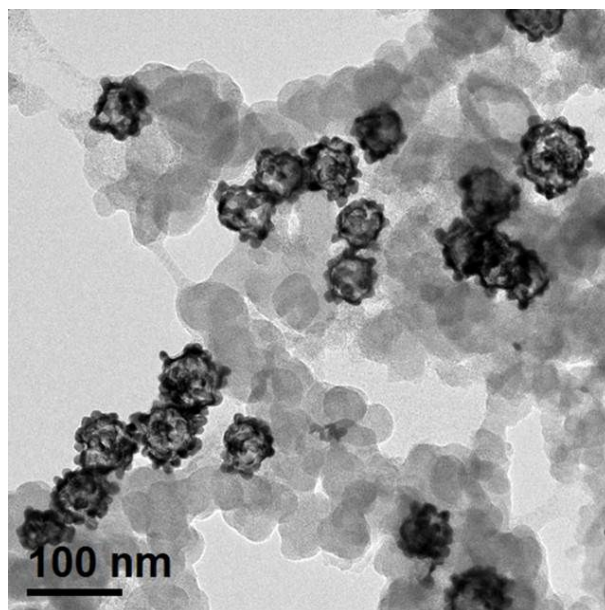


Figure S13. Low magnification TEM image of hollow Pt-Ni-Co NDs after supporting on commercial carbon powder.

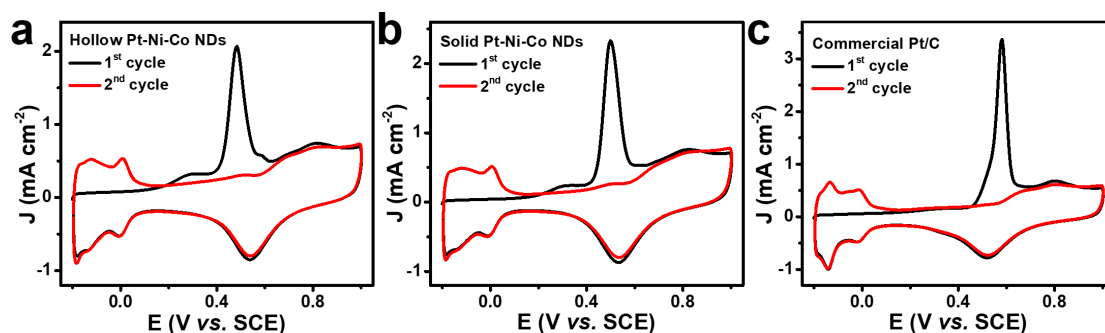


Figure S14. The first and second cycle of CO-stripping voltammograms for: a) hollow Pt-Ni-Co NDs, b) solid Pt-Ni-Co NDs and c) commercial Pt/C. The current densities were normalized by the surface area of working electrode.

The $ECSA_{CO}$ are determined by integrating CO oxidative charge of the first cycle stripping. The calculated $ECSA_{CO}$ of hollow Pt-Ni-Co NDs, solid Pt-Ni-Co NDs and commercial Pt/C are 50.60, 22.53 and 29.66 $m^2 g^{-1}_{Pt}$, respectively. It can be found that the $ECSA_{CO}$ value of the three catalysts show similar trend, which is consistent with that of $ECSA_H$.

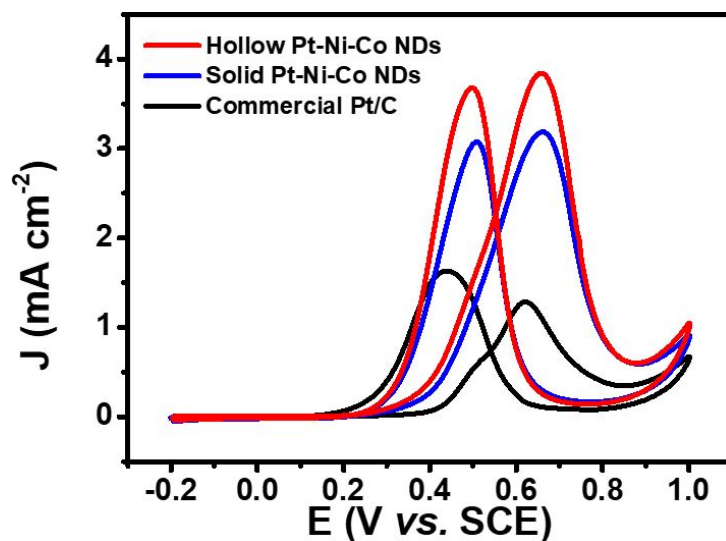


Figure S15. Specific activities of hollow Pt-Ni-Co NDs, solid Pt-Ni-Co NDs and commercial Pt/C recorded in 0.5 M H_2SO_4 + 1.0 M CH_3OH . The sweep rate is 50 mV s^{-1} .

The specific activity of hollow Pt-Ni-Co NDs is 3.8 mA cm^{-2} , which is 0.7 and 2.9 times greater than that of solid Pt-Ni-Co NDs and Pt/C, respectively.

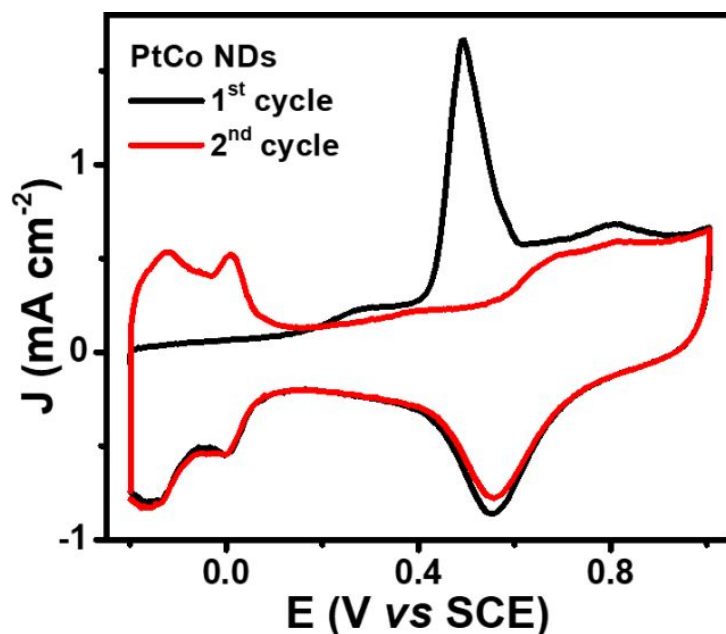


Figure S16. The first and second cycle of CO-stripping voltammogram for synthesized Pt-Co NDs. The current density was normalized by the surface area of working electrode.

To further understand the influence of Co for the enhanced CO tolerance, CO stripping tests on Pt-Co NDs were carried out. The Pt-Co NDs were synthesized by using the standard procedure but without Ni precursors. It was found that the peak potential of CO oxidation on Pt-Co NDs is much more negative than that on Pt/C, implying the much enhanced CO tolerance. This should be attributed to the additional oxygen source for the oxidation of CO or CO-like intermediates introduced by the introduction of Co elements.

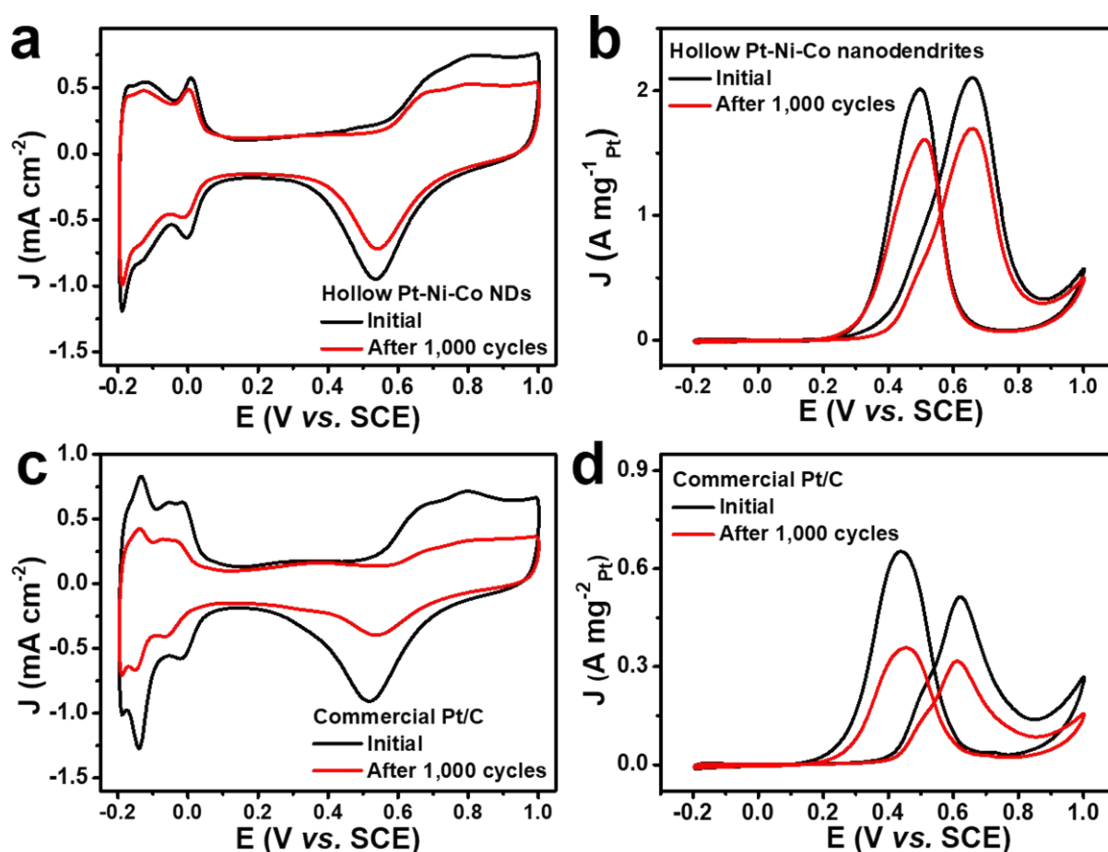


Figure S17. The stability test of hollow Pt-Ni-Co NDs and commercial Pt/C recorded in (a, c) 0.5 M H₂SO₄, and (b, d) in 0.5 M H₂SO₄ + 1.0 M CH₃OH. The scan rate was 50 mV s⁻¹.

After scanning 1,000 cycles in 0.5 M H₂SO₄ + 1.0 M CH₃OH, the ECSA_H of hollow Pt-Ni-Co NDs and commercial Pt/C remain 79% and 49% of their initial value, respectively. The mass activity of hollow Pt-Ni-Co NDs is reduced by 19%, while that of commercial Pt/C is decreased by 38%.

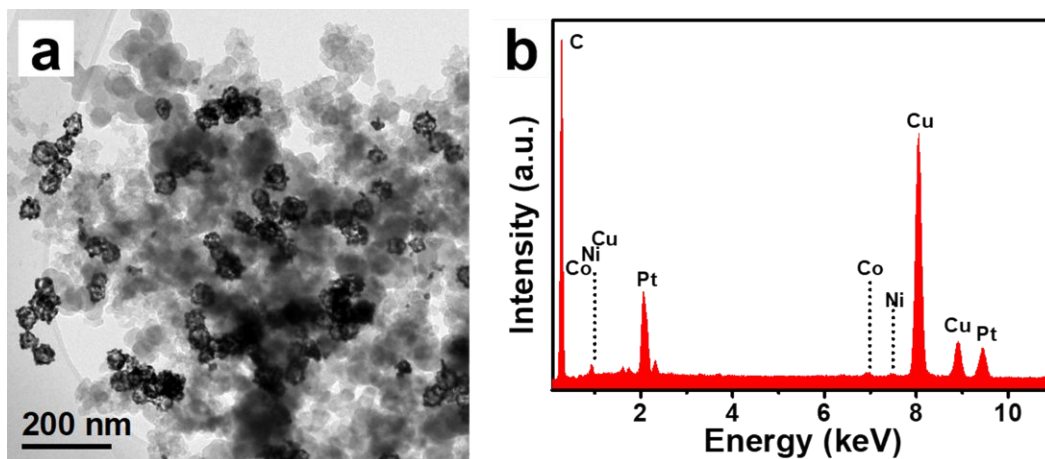


Figure S18. (a) low magnification TEM image and (b) EDS analysis of hollow Pt-Ni-Co NDs after scanning 1,000 cycles in 0.5 M H₂SO₄ + 1.0 M CH₃OH.

As shown in figure S18, the morphology and composition of hollow Pt-Ni-Co NDs after durability test are characterized. The structure of hollow Pt-Ni-Co NDs are largely maintained. The slight decrease of Ni and Co results from electrochemical de-alloy during durability test.

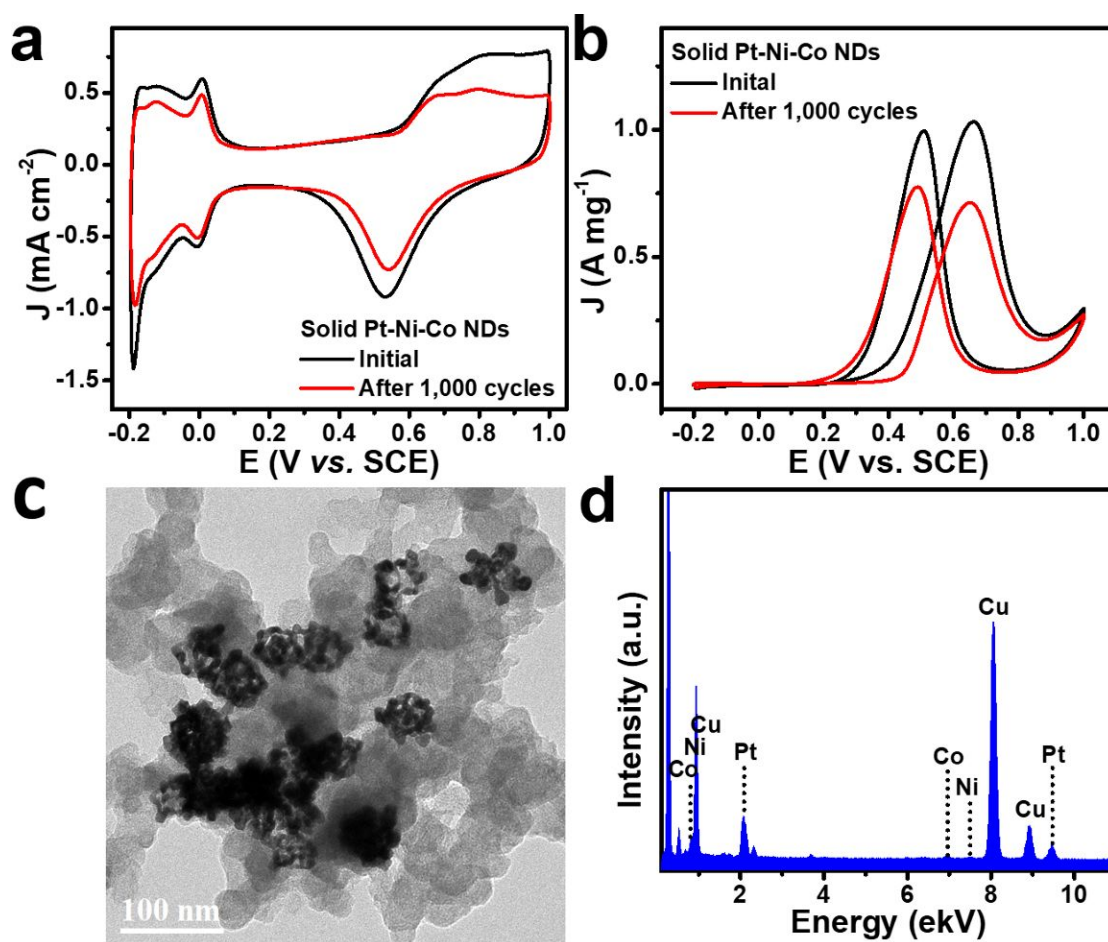


Figure S19. The stability test of solid Pt-Ni-Co NDs recorded in (a) 0.5 M H₂SO₄ and (b) in 0.5 M H₂SO₄ + 1.0 M CH₃OH. The scan rate was 50 mV s⁻¹. (c) TEM image and (d) EDS analysis of solid Pt-Ni-Co NDs after scanning 1,000 cycles.

Figure S19 demonstrates the durability test of solid Pt-Ni-Co NDs. After scanning 1,000 cycles in 0.5 M H₂SO₄ + 1.0 M CH₃OH, the ECSA_H and mass activity of solid Pt-Ni-Co NDs are 23.7 m² g⁻¹_{Pt} and 0.71 A mg⁻¹_{Pt}, which are decreased to 73% and 69% of the initial value. Solid Pt-Ni-Co NDs after electrochemical tests was collected and investigated. It was found that solid structure was transformed to hollow structure, and element component of Pt-Ni-Co are changed from 24:66:10 to 72:16:12, indicating the structure of solid Pt-Ni-Co NDs are not stable under acidic condition.

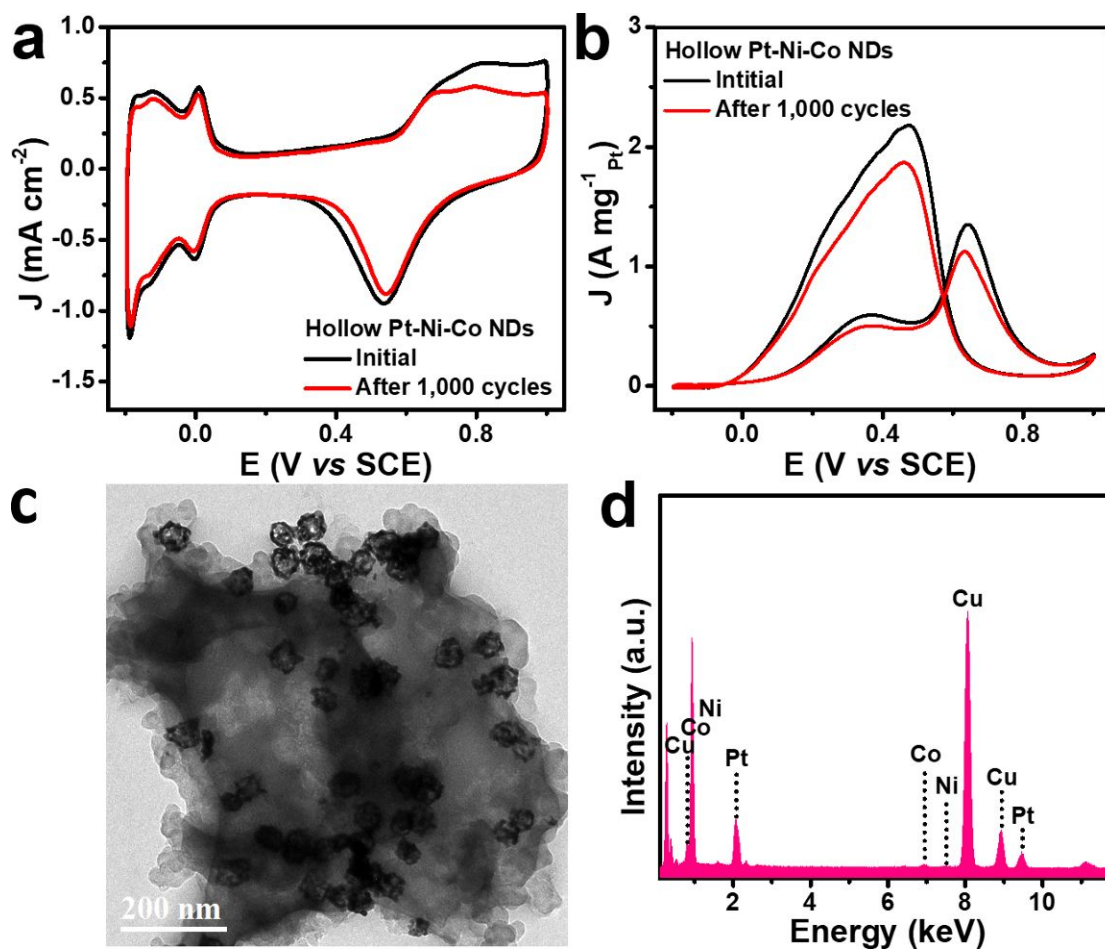


Figure S20. The stability test of hollow Pt-Ni-Co NDs recorded in (a) 0.5 M H₂SO₄, and (b) in 0.5 M H₂SO₄ + 0.25 M HCOOH. The scan rate was 50 mV s⁻¹. (c) TEM image and (d) EDS analysis of hollow Pt-Ni-Co NDs after scanning 1,000 cycles in 0.5 M H₂SO₄ + 0.25 M HCOOH.

We performed the stability tests for formic acid oxidation reaction (FAOR) by scanning 1,000 cycles in 0.5M H₂SO₄+ 0.25 M HCOOH, and then collected catalysts to investigate their chemical composition.

As shown in Figure S20, the ECSA_H and mass activity @0.4 V of hollow Pt-Ni-Co NDs after tests are 21.85 m² g⁻¹_{Pt} and 0.5 A mg⁻¹_{Pt}, which are approximately 88% and 86% of their initial value, respectively. Moreover, the chemical composition was changed from Pt₆₅Ni₁₇Co₁₈ to Pt₇₂Ni₁₂Co₁₆, as revealed by EDS. Therefore, the hollow Pt-Ni-Co NDs exhibit better stability for FAOR than MOR. This should be ascribed to the suppression of formic acid for the leaching process.

References

1. Fu, G., Liu, H., You, N., Wu, J., Sun, D., Xu, L., Tang, Y., Chen, Y., Dendritic platinum-copper bimetallic nanoassemblies with tunable composition and structure: Arginine-driven self-assembly and enhanced electrocatalytic activity. *NANO RES.* **2016**, 9(3), 755-765.
2. Fu, G., Zhang, Q., Wu, J., Sun, D., Xu, L., Tang, Y., Chen, Y., Arginine-mediated synthesis of cube-like platinum nanoassemblies as efficient electrocatalysts. *NANO RES.* **2015**, 8(12), 3963-3971.
3. Yu, X., Wang, D., Peng, Q., Li, Y., High performance electrocatalyst: Pt-Cu hollow nanocrystals. *Chem Commun.* **2011**, 47(28), 8094-8096.
4. Oh, A., Baik, H., Choi, D.S., Cheon, J.Y., Kim, B., Kim, H., Kwon, S.J., Joo, S.H., Jung, Y., Lee, K., Skeletal octahedral nanoframe with cartesian coordinates via geometrically precise nanoscale phase segregation in a Pt@Ni core-shell nanocrystal. *ACS nano.* **2015**, 9(3), 2856-2867.
5. Zheng, Y., Zeng, J., Ruditskiy, A., Liu, M., Xia, Y., Oxidative etching and its role in manipulating the nucleation and growth of noble-metal nanocrystals. *Chem. Mater.* **2013**, 26(1), 22-33.
6. Dong, J., Song, L., Yin, J.J., He, W., Wu, Y., Gu, N., Zhang, Y., Co₃O₄ nanoparticles with multi-enzyme activities and their application in immunohistochemical assay. *ACS Appl. Mater. Interfaces.* **2014**, 6(3), 1959-1970.
7. Zhang, L., Zhang, X.F., Chen, X.L., Wang, A.J., Han, D.M., Wang, Z.G., Feng, J.J., Facile solvothermal synthesis of Pt₇₁Co₂₉ lamellar nanoflowers as an efficient catalyst for oxygen reduction and methanol oxidation reactions. *J. Colloid Interface Sci.* **2019**, 536, 556-562.